Atmos. Chem. Phys. Discuss., 15, 7057–7087, 2015
www.atmos-chem-phys-discuss.net/15/7057/2015/
doi:10.5194/acpd-15-7057-2015

Atmospheric Chemistry and Physics Discussions

Influence of the aerosol solar extinction on photochemistry during the 2010 Russian wildfires episode

J. C. Péré[1], B. Bessagnet[2], V. Pont[3], M. Mallet[3], and F. Minvielle[1]

[1]Laboratoire d'Optique Atmosphérique, Université Lille 1, 59655 Villeneuve d'Ascq, France
[2]Institut National de l'Environnement Industriel et des Risques, Parc Technologique Alata, 60550 Verneuil en Halatte, France
[3]Laboratoire d'Aérologie, Observatoire Midi-Pyrénées, 14 Avenue Edouard Belin, 31400 Toulouse, France

Received: 17 November 2014 – Accepted: 13 February 2015 – Published: 10 March 2015

Correspondence to: J. C. Péré (jean-christophe.pere@univ-lille1.fr)

Published by Copernicus Publications on behalf of the European Geosciences Union.

Abstract

In this work, impact of aerosol solar extinction on the photochemistry over eastern Europe during the 2010 wildfires episode is discussed for the period from 5 to 12 August 2010, which coincides to the peak of fire activity. The methodology is based on an on-line coupling between the chemistry-transport model CHIMERE (extended by an aerosol optical module) and the radiative transfer code TUV. Results of simulations indicate an important influence of the aerosol solar extinction, in terms of intensity and spatial extent, with a reduction of the photolysis rates of NO_2 and O_3 up to 50 % (in diurnal-averaged) along the aerosol plume transport. At a regional scale, these changes in photolysis rates lead to a 3–15 % increase in the NO_2 daytime concentration and to an ozone reduction near the surface of 1–12 %. The ozone reduction is shown to occur over the entire boundary layer, where aerosols are located. Also, comparisons of simulations with air quality measurements over Moscow show that the inclusion of the aerosol feedback tends to slightly improve performance of the model in simulating NO_2 and O_3 ground concentrations. In term of air quality prediction, the O_3 peak reduction when including aerosol feedback results in a non-negligible difference in the predicted exceedance of alert threshold compared to the simulation without aerosol feedback, in coherence with measurements. Finally, the total aerosol mass concentration (PM_{10}) is shown to be decreased by 1–2 %, on average during the studied period, caused by a reduced formation of secondary aerosols such as sulphates and secondary organics (4–10 %) when aerosol impact on photolysis rates is included.

1 Introduction

For several years, it has been well recognized that air pollution of gaseous and particulate origin can have adverse health effects (Miller et al., 2012; Beelen et al., 2014). In consequence, efficient air pollution control strategies have now become a challenge for environmental policies. In the context of air quality monitoring, the exceed of cer-

ACPD
15, 7057–7087, 2015

tain thresholds of pollutant concentrations is a criterion often used by authorities of a country to prevent people from air pollution exposure. In general, the exceed of these thresholds is evaluated from air quality numerical forecast such as in France where the regional chemistry-transport model CHIMERE (Menut et al., 2013) is used in the French national air quality forecasting and monitoring system known as PREV'AIR (Honoré et al., 2008). Photochemical pollutants (ozone, secondary aerosols,. . .), which are formed from photo-dissociation of precursors such as nitrogen dioxide (NO_2) and volatile organic compounds (VOC) (Jenkin and Clemitshaw, 2000), are of particular interest for air quality monitoring (Honoré et al., 2008) due to their negative impacts on both environment and human health (Amin, 2014; Hunova et al., 2014).

The key parameter that governs the photo-dissociation of photochemical precursors in the atmosphere is the photolysis rate, which mainly depends on the available actinic flux (Seinfeld and Pandis, 2006). Aerosols are known to have large influence on the available actinic flux by interacting with solar radiation in the ultraviolet-visible wavelengths (Li, J. et al., 2011; Li, G. et al., 2011; Lou et al., 2014). For example, Wai and Tanner (2010) showed, by using a combination of remote sensing observations and chemical-transport model, that aerosol solar extinction could lead to a 7–32 % reduction in maximum ozone concentration over Hong-Kong during highly polluted days. Also, Li, G. et al. (2011) highlighted, with WRF-CHEM modelling experiments, that changes in photolysis rates due to the presence of particles led to a decrease of about, respectively, 2–17 and 5–6 % in daytime ozone and secondary aerosols (nitrate, secondary organics) concentrations over Mexico City during the 2006 Megacity Initiative: Local and Global Research Observations (MILAGRO) campaign.

To reduce computational time for operational purpose, one major characteristic of air quality modelling platforms is that impacts of aerosols and clouds on solar radiation are often taken into account as simplified attenuation factors when evaluating the photolysis rates (Honoré et al., 2008; Menut et al., 2013). However, Real and Sartelet (2011) highlighted that simplified parametrization of aerosol impact on photolysis rates

ACPD
15, 7057–7087, 2015

could tend to worsen air quality model performance in simulating ozone and particulate concentration, especially under highly polluted environments.

The aim of the present study is to implement, in the chemistry-transport model CHIMERE, an explicit representation of the alteration of photolysis rates by aerosols and discuss the impact in terms of modelled ozone budget and the formation of secondary aerosols at regional scale. We emphasize on a major fire event that occurred in Russia during August 2010 as its episode was characterized by important concentrations of primary and secondary aerosols and large concentrations of ozone, especially over this specific region (Zvyagintsev et al., 2010; Konovalov et al., 2011; Popovicheva et al., 2014). Then, it represents an excellent opportunity to discuss how aerosol solar extinction can affect photochemistry. The approach is based on an on-line coupling between the regional model CHIMERE, extended by an aerosol optical module (Péré et al., 2010), and the Tropospheric Ultraviolet and Visible (TUV) radiation model (Madronich and Flocke, 1998). In this methodology, the aerosol optical thickness, single scattering albedo and asymmetry parameter are first modelled by CHIMERE using an aerosol core-shell mixing hypothesis, as in Péré et al. (2009, 2010). This mixing approach has been previously used by Péré et al. (2014) to study the 2010 Russian wildfires direct radiative forcing and its feedback on the regional atmospheric dynamics. Results indicate that it can give a good representation of the absorption properties of particles during this specific period. In a second time, aerosol optical properties are used as inputs in the radiative transfer code TUV to evaluate the impact of aerosol short-wave solar extinction on photolysis rates and the formation of ozone and secondary particles. The advantage of such methodology is the use of two specific state-of-the-art models to explicitly simulate the interaction of physico-chemically resolved aerosols with the actinic flux and the associated impact on modelled photolysis rates and photochemistry.

Section 2 describes the configuration of each model as well as the development of their on-line coupling. In Sect. 3 are discussed modelled regional changes in the near surface concentrations of NO_2, O_3 and secondary aerosols over Russia induced

ACPD
15, 7057–7087, 2015

by modifications of photolysis rates by smoke aerosols during August 2010. Finally, conclusions and perspectives of future works are given in Sect. 4.

2 Methodology

2.1 Description of the CHIMERE model

2.1.1 Aerosol module

CHIMERE is a state-of-the-art 3-D chemistry transport model that calculates the concentrations of numerous gaseous and particulate pollutants (Vautard et al., 2001; Menut et al., 2013). The dynamics and gas phase parts of the model is regularly improved (Menut et al., 2013) and its documentation can be downloaded at http://www.lmd.polytechnique.fr/chimere/. In this work, the CHIMERE domain has a 30 km horizontal resolution and ranges from 43.40 to 63.20° N in latitude and from 18.70 to 57.30° E in longitude. The aerosol part is described by Bessagnet et al. (2004) and is composed of 10 chemical species: sulphates, nitrates, ammonium, primary organic and black carbon (OC and BC), secondary organic aerosols (SOA), sea salt, natural and anthropogenic dust and water. The evolution of aerosols is described with a 8-bins size distribution (from about 40 nm to 10 µm in diameter) and includes the main physical processes such as nucleation, coagulation, condensation/evaporation, adsorption/desorption, wet and dry deposition and scavenging.

Anthropogenic emissions of gaseous and particulate origin come from the EMEP database. Concerning OC and BC emissions, the inventory of Junker and Liousse (2008) has been used. Natural soil dust are dynamically produced within the domain according to the methodology of Vautard et al. (2005). SOA formation is represented through oxidation processes of relevant precursors of biogenic and anthropogenic origin and gas particle partitioning schemes (Bessagnet et al., 2008). VOC and NO emissions from vegetation are calculated using the Model of Emissions of Gases and

ACPD
15, 7057–7087, 2015

Aerosols from Nature (MEGAN) (Guenther et al., 2006). Aerosols and gases emitted by wildfires affecting Russia during 2010 are taken into account following the work described and validated by Kaiser et al. (2012). It consists in the assimilation of the fire radiative observations from the Moderate Resolution Imaging Spectroradiometer into the Global Fire assimilation System combined with the use of specific combustion rate and emission factors to estimate biomass burning emissions. More information on the methodology as well as a validation study for the 2010 Russian wildfires episode can be found in (Kaiser et al., 2012).

CHIMERE is forced at these boundaries by monthly climatologies, calculated over the 2000–2004 period, of the main gases and particles provided by the MOZART (Horowitz et al., 2003) and LMDzT–INCA global chemistry-transport models (Hauglustaine et al., 2004), respectively. Also, CHIMERE is off-line driven by the Weather Research and Forecasting model (WRF) at a 30 km resolution.

2.1.2 Modelling aerosol optical properties

The calculation of optical properties of particles is the pre-requisite for the evaluation of their impacts on photolysis rates and photochemistry as they provide information on how aerosols will interact with the actinic flux. In that sense, we developed a numerical scheme dedicated to calculate aerosol optical properties from aerosol concentrations, size distribution and chemical composition modelled by CHIMERE. A complete description of this optical module is presented in the work of Péré et al. (2010). To compute the complex refractive index of a particle, the hypothesis of a core-shell mixing has been chosen with a core of primary species (BC, OC and dust) surrounded by a shell of secondary ones (sulphates, nitrates, ammonium, secondary organics) and sea salt and water. This mixing choice is supported by recent studies giving evidence of coatings of secondary particles on black carbon aerosols over Europe (Vester et al., 2007; McMeeking et al., 2011). Also, such mixing has been shown to correctly reproduce the absorbing properties of aerosols during the 2010 Russian wildfire episode (Péré et al., 2014). For each size bin, a volume average procedure is used to calculate the refrac-

ACPD
15, 7057–7087, 2015

tive index of the core and the shell (Lesins et al., 2002) which is then used as inputs in the Mie algorithm for *n*-layered spheres of Wu and Wang (1991) to calculate the scattering and absorption coefficients. It should be noted that the volume of the core and the shell can vary during the simulation in function of the different physical processes influencing aerosol population. The optical properties of the total aerosol distribution needed in radiative transfer modelling, such as the Aerosol Optical Thickness (AOT), Single Scattering Albedo (SSA) and asymmetry parameter (g), are calculated as in Wu et al. (1996).

A detailed evaluation of the optical module for the 2010 Russian wildfire episode by using Aerosol Robotic Network (AERONET) sunphotometers measurements (AOT, SSA, aerosol size distribution) and Polarization and Directionality of the Earth's Reflectances (POLDER) and Cloud-Aerosol LIdar with Orthogonal Polarization (CALIOP) aerosol extinction data is presented by Péré et al. (2014). Only a sum-up is given here. As displayed in Fig. 1a and b, simulations for the period 5–12 August 2010 (peak of fire activity) show large AOT (at midday) over eastern Europe with modelled values above 2 (at 400 nm) in the aerosol plume. This aerosol plume was transported in an anticyclonic flow from the source region towards Moscow (5–8 August), to the north (9–10 August) and then back to the east (11–12 August). On average, simulations compare well with AOT POLDER data in terms of spatial distribution and intensity (correlation = 0.67–0.77, $-10\,\% <$ biases $< 23\,\%$). The altitude of transport was shown to be below 5 km and comparisons between CHIMERE and CALIOP show good consistency. Figure 1a and b indicates that the simulated plume was advected over Moscow between 5–9 August, which is in accordance with AERONET measurements. During the study period, the aerosol composition was dominated by scattering organic species with modelled elevated SSA (0.97 between 300 and 1000 nm) close to AERONET values over Moscow (0.95–0.96 between 440 and 1020 nm). Globally, the comparisons between aerosol simulation and sunphotometers data highlighted the ability of the model to give an appropriate representation of the aerosol size distribution and scattering/absorption

ACPD
15, 7057–7087, 2015

properties (Péré et al., 2014), which is the pre-requisite to evaluate its influence on photolysis rates and the formation of photochemical pollutants.

2.2 Description of the TUV model

TUV is a widely-used state-of-the-art radiative transfer model developed at the National Centre for Atmospheric Research (Madronich and Flocke, 1998). In this study, we used the version 4.6 of the code (released in March 2009) freely available at the website: http://cprm.acd.ucar.edu/Models/TUV/. The model calculates the actinic flux and photolysis rates of a large number of photochemical species.

Photolysis is the process breaking the covalent bond of some reactive gaseous species by short-wave solar radiation. This process is very important in the atmosphere as it controls the abundance of numerous air pollutants such as ozone and nitrogen dioxide. The photolysis rate of a given specie J (s^{-1}) is calculated as follows:

$$J(s^{-1}) = \int_{\lambda_1}^{\lambda_2} \sigma(\lambda,T) \cdot \phi(\lambda,T) \cdot F(\lambda) \mathrm{d}\lambda \quad (1)$$

where $\sigma(\lambda,T)$ and $\phi(\lambda,T)$ are, respectively, the absorption cross section (cm^2) and the quantum yield of a given molecule, T the air temperature (K) and $F(\lambda)$ the actinic flux between wavelengths λ_1 and λ_2 (photons $cm^{-2}\,s^{-1}\,nm^{-1}$). The absorption cross section reflects the probability of collision between a photon and the molecule, while the quantum yield is the probability that the molecule is dissociated after collision with a photon. The dependence of both parameters on the air temperature is calculated by TUV by using the vertical profile of air temperature issued from the meteorological model WRF used to drive CHIMERE.

The actinic flux is calculated by integrating the solar flux over all sphere angles considering 5646 wavelengths between 120 and 1250 nm. When going through the atmosphere, the actinic flux can be attenuated by molecular absorption and diffusion but

ACPD
15, 7057–7087, 2015

also by the presence of clouds and aerosols. For clouds and aerosols, the attenuation is calculated by using their respective aerosol optical thickness, single scattering albedo and asymmetry parameter. In TUV, three types of clouds are represented: low, middle and high altitude clouds. Altitudes of their bases and tops as well as their optical thicknesses are estimated by the meteorological model WRF. The single scattering albedo and asymmetry parameter are considered constant in the UV–visible wavelengths and are taken equal to, respectively, 0.99 and 0.85 for the three types of clouds (Madronich and Flocke, 1998). It should be noted that changes in the cloud optical properties due to the activation of aerosols into cloud condensation nuclei are not taken into account in our approach. However, the anticyclonic conditions that prevailed over eastern Europe during the studied period suggest a low impact of clouds on the modelled actinic flux and photolysis rates (Lau and Kim, 2012).

Concerning aerosols, the three optical properties (AOT, SSA and g) are calculated at 200, 300, 400, 500, 600 and 700 nm using the aerosol optical module and then interpolated to the TUV wavelength grid (120–1250 nm). To solve the radiative transfer equation and compute the actinic flux along the atmospheric column, the Eddington approximation has been chosen in TUV as it allows an accurate estimation of modelled radiative fluxes (Joseph et al., 1976).

2.3 On-line coupling between CHIMERE and TUV

The methodology developed in this study consists of a one-way and on-line coupling between TUV and CHIMERE. In this approach, the radiative transfer code TUV has been implemented within CHIMERE so that each model runs simultaneously. During the simulation, the aerosol optical properties modelled by CHIMERE for a core-shell mixing (AOT, SSA, g) are used as inputs in TUV in order to take into account the influence of aerosol solar extinction on photolysis rates. Then, the photolysis rates estimated by TUV are in turn used by CHIMERE to calculate the concentrations of photochemical pollutants.

Two simulations are performed for the period of peak fire activity (5–12 August 2010):

ACPD
15, 7057–7087, 2015

1. In the first one, the attenuation of actinic flux is only due to gases and clouds: CHIMERE–TUV(gases+clouds).

2. In the second one, the impact of aerosols on solar extinction is added in the photolysis rates calculation: CHIMERE–TUV(gases+clouds+aerosols).

The impact of aerosols on photolysis rates and associated concentrations of photochemical pollutants are then estimated by differentiating the two simulations: (2) – (1).

We will focus on the aerosol impact on NO_2 and O_3 photolysis rates, which mainly drives the concentration of ozone, NO_2 and OH radicals in the troposphere. Indeed, the major source of ozone is the result of the NO_2 photolysis:

$$NO_2 + \hbar \cdot \vartheta \longrightarrow NO + O(^3P) \quad J[NO_2] \tag{R1}$$

followed by the reaction of $O(^3P)$ with a dioxygene molecule (M is a third body favouring the reaction):

$$O(^3P) + O_2 + M \longrightarrow O_3 + M \tag{R2}$$

Given that Reaction (R2) is rapid, the formation rate of ozone is mainly determined by the constant rate $J[NO_2]$. In parallel, the major sink of ozone during daytime is its photo-dissociation following the reaction:

$$O_3 + \hbar \cdot \vartheta \longrightarrow O_2 + O(^1D) \quad J[O_3] \tag{R3}$$

$O(^1D)$ will rapidly react with a water molecule to form OH radicals:

$$O(^1D) + H_2O \longrightarrow 2OH \tag{R4}$$

The latter reaction is a major source of OH radicals in the troposphere. They are involved in the formation of secondary particles as oxidants of their gaseous precursors. For example, they contribute to the oxidation of SO_2, NO_2 and COV, which can result in the formation of, respectively, sulphate, nitrate and secondary organic aerosols.

ACPD
15, 7057–7087, 2015

3 Results and discussion

3.1 Regional impact of the 2010 Russian wildfires on the formation of ozone and nitrogen dioxyde

During the wildfire episode, the important concentrations of scattering aerosols have affected significantly the UV-visible solar radiation in terms of intensity and spatial extent. Figures 2a, b and 3a, b report the diurnal-averaged percentage changes in near surface photolysis rates of NO_2 and O_3, respectively. Changes are shown to be negative over the entire area with mean diurnal values between −2 and −50 % and closely follow the AOT spatial features (see Fig. 1a and b). It is interesting to note that the impact of the aerosol solar extinction is more pronounced for $J[O_3]$ than for $J[NO_2]$, for each day of the studied period. For both photolysis rate, the largest reduction is simulated along the transport of the aerosol plume (20–50 %). The photochemistry over the Moscow region has also been affected, especially during the arrival of the aerosol plume between 6 and 10 August 2010. This point will be discussed in further details hereafter. These modelled changes obtained here are comparable with the recent study of Real and Sartelet (2011) in which they simulate, by using the chemistry-transport model Polyphemus-Polair3D coupled with the radiative transfer code Fast-J, a reduction of $J[NO_2]$ and $J[O_3]$ reaching 30 % (in monthly mean) during summer 2001 over European regions characterized by elevated AOT (0.6–0.7 at 550 nm). Also, Hodzic et al. (2007) simulated a 15–30 % NO_2 photolysis reduction during the 2003 European summer heatwave in case of absorbing biomass burning aerosols (AOT(550 nm) = 0.7–0.8, SSA (532 nm) = 0.83–0.87).

According to Reactions (R1)–(R3), the alteration of $J[NO_2]$ and $J[O_3]$ in the presence of aerosols suggests, in turn, a modification of their concentrations near the surface. Figure 4 gives an example of these corresponding changes during the 8 August for NO_2 and O_3. Some notable modification of the NO_2 concentration is simulated, as it is mainly driven during daytime by its photolytic destruction (see Reaction R1). The important diminution of $J[NO_2]$ due to aerosols (between 2 and 50 %) leads to an in-

ACPD
15, 7057–7087, 2015

crease of its near surface concentration reaching, in average, 3 to 15 %. Concerning ozone, its daytime concentration is influenced by both variations of $J[NO_2]$ (source of ozone, see Reactions R1 and R2) and variations of $J[O_3]$ (sink of ozone, see Reaction R3). We can deduce from Fig. 4 that the influence of $J[NO_2]$ reduction seems to slightly dominate the influence of $J[O_3]$ reduction, resulting in a decrease of the near surface concentration of ozone between 1 and 12 %. These results are comparable to those obtained by Real and Sartelet (2011) who simulated a 4–8 % reduction of near-surface ozone concentration (for July 2001) over areas where the decrease of $J[NO_2]$, due to the aerosol solar extinction, reached 30 %. Also, Mena-Carrasco et al. (2009) highlighted, by combining STEM-2K3 model experiments and aircraft observations from the MILAGRO campaign during March 2006, a 40 % attenuation of $J[NO_2]$ associated to an intense aerosol plume over Mexico City, resulting in a 5–10 % diminution of ozone production. Such impacts are however less pronounced than the ones obtained over some highly polluted Asian regions. For example, Bian et al. (2007) and Wai and Tanner (2010) showed, over China, a reduction of maximum ozone concentration reaching 30 to 70 % associated to similar aerosol loadings as obtained in our study ($1 < AOT(550\ nm) < 2.5$). The low absorbing properties of the Russian smoke plume (Péré et al., 2014) could be a reason for such a behaviour.

To further investigate aerosol feedback on the ozone cycle and the formation of secondary particles, we will now focus our study on the Moscow region where the aerosol solar extinction is pronounced, especially during the aerosol plume overpass (5–9 August 2010). Gaseous and particulate measurements from the Moscow air quality station will also be used in the analysis.

3.2 Impact of the 2010 Russian wildfires on the photochemistry over Moscow

On Fig. 5, the impact of particles on the formation of ozone and nitrogen dioxide over Moscow is discussed in terms of percentage changes (at midday) in their near-surface photolysis frequencies and concentrations as a function of modelled AOT (440 nm). As expected, changes appear to have a good linearity with AOT (440 nm) with a correla-

ACPD
15, 7057–7087, 2015

tion of 0.96–0.98, i.e. modifications become more important when the aerosol loading increases. As shown previously over the entire area, $J[O_3]$ is more sensitive to the presence of particles (reduction of about 19 % per unit of AOT) than $J[NO_2]$ (reduction of about 10 % per unit of AOT). These modifications of photolysis rates result in an increase of the ground NO_2 concentration of 4 % (per unit of AOT) and a small reduction of ground O_3 of 2 % (per unit of AOT). It should be noted that changes modelled here at midday are less important than regional changes previously obtained in diurnal-mean (see Figs. 2a, b, 3a, b and 4) as the optical path (and then interaction of aerosols with solar radiation) is minimum at midday, compared to the rest of the day.

The influence of aerosols on photochemistry does not only occur at the surface but also in the low troposphere, as illustrated in Fig. 6. This Figure presents the vertical profile of the diurnal-averaged percentage changes in the ozone concentration at the north of Moscow (59.9° N, 37.6° E) for the 9 August. The aerosol extinction coefficient (in km^{-1}) modelled by CHIMERE and measured by CALIOP at midnight is also indicated. The maximum ozone reduction (4–5 %) occurred below the two first km of the atmosphere within the aerosol plume (modelled extinction of 0.50–0.95 km^{-1}). Above, the influence of aerosols on the ozone formation gradually decrease to become negligible at an altitude of 5–6 km. It should be noted that below an altitude of 2 km (where more that 70 % of the aerosol solar extinction occurs), the modelled aerosol extinction is within the uncertainty range of CALIOP measurements, giving confidence in the estimated impact of aerosols on the ozone reduction.

In terms of model performance, it is interesting to see if an explicit representation of aerosol impact on photolysis rates tend to improve the simulation of the concentration of photochemical pollutants, compared to a simulation without aerosol feedback. For such analyse, statistical comparisons between the near-surface concentrations of NO_2 and O_3 simulated with and without aerosols and measured at Moscow by an air quality station has been made. Results are presented in Tables 1 and 2 for hourly values and daily maximum values, respectively. We can see that, for both configurations, scores for ozone and NO_2 are much lower than the ones usually obtained over western Eu-

ACPD
15, 7057–7087, 2015

rope with the CHIMERE model (Honoré et al., 2008), with RMSE of 48–88 $\mu g\,m^{-3}$ and correlation of 0.22–0.60. A possible reason could be that the EMEP emission database used in this study is less well documented for eastern Europe. However, Tables 1 and 2 indicates that the inclusion of aerosols in the simulation improves the correlation and slightly reduces biases with measurements for both species and for both hourly and maximum values.

To further investigate the aerosol feedback on the ozone diurnal cycle, Fig. 7 displays the temporal evolution (between 5 and 12 August 2010) of the near-surface ozone concentration (in $\mu g\,m^{-3}$) modelled with and without aerosol feedback along with corresponding observations at the Moscow monitoring station. The European alert threshold of 240 $\mu g\,m^{-3}$ is also indicated by a straight line. First, Fig. 7 confirms the moderate overall impact of the aerosol solar extinction on the ozone production, with a maximum diminution reaching 7–10 % during the aerosol plume overpass (7, 8 and 9 August), which leads to slightly reduce the bias between model and observations. For the other days, the alteration of photolysis rates by aerosols is also present but a similar impact on both the sink and source of ozone is simulated, leading to a negligible impact on the ozone production. Depending on the day, the model simulates lower or higher hourly values compared to observations. As indicated previously, uncertainties on the EMEP emission database for this specific region could be a possible reason for these biases. Also, the model is shown to overestimate nighttime concentrations over the period, which could be due to uncertainties in correctly estimating its dry deposition and titration by NO, as previously highlighted by Honoré et al. (2008) over Western Europe. It should be noted that a inadequate representation of the nocturnal air ventilation could also be a reason for such a model bias. Second, Fig. 7 indicates that the European alert threshold of 240 $\mu g\,m^{-3}$ is predicted to be exceeded during 8 August 2010 for the simulation without aerosol impacts, with a maximum modelled concentration reaching 251 $\mu g\,m^{-3}$ in the middle of the afternoon. However, this limit is not exceeded when considering aerosol feedback effects with a reduction of the modelled ozone peak from 251 to 230 $\mu g\,m^{-3}$, in coherence with observations (160 $\mu g\,m^{-3}$). Hence, taking into

ACPD
15, 7057–7087, 2015

account the impact of aerosol solar extinction on photolysis rates in the CHIMERE numerical simulations could play a non-negligible role in term of air quality prediction, keeping in mind that better constrained emissions and nocturnal processes could also greatly improve model scores.

In parallel, the presence of aerosols tends to reduce the oxidising capacity of the atmosphere (through reduction of OH radicals, see Reaction R4), which leads to decrease the formation of secondary aerosols. As illustrated in Fig. 8, the maximum reduction in the near-surface concentrations of sulphates (oxidation product of SO_2) and SOA (oxidation product of COV) occurs on 9 August with diurnal-averaged values of 10 and 4 %, respectively. The overall impact is then a slightly reduction of the total aerosol mass concentration (PM_{10}) comprised between 1 and 2 % over the entire period. These results are comparable to the findings of Real and Sartelet (2011) and Li, G. et al. (2011) who showed a 5–10 % reduction of the formation of secondary aerosols due to the aerosol solar extinction, in case of intense particulate pollution over, respectively, Europe and Mexico City.

4 Conclusions

In the present study, we have developed an on-line coupling between the chemistry-transport model CHIMERE (complemented by an aerosol optical module) and the radiative transfer code TUV to study the impact of aerosol solar extinction on the photochemistry over eastern Europe during the 2010 wildfires episode. Simulations from 5 to 12 August 2010, corresponding to the peak of fire activity, have been performed with and without aerosol impact on photolysis rates and concentrations of gaseous and particulate pollutants. Large areas was affected by important concentrations of particles, with modeled AOT (440 nm) above 2 along the transport of the aerosol plume. A previous evaluation of the modeled optical properties during this specific episode (Péré et al., 2014) showed good model performance in simulating both the magnitude and spectral dependence of the aerosol optical thickness and single scattering albedo.

ACPD
15, 7057–7087, 2015

The impact of aerosols on photolysis rates is shown to be regionally significant with a mean reduction of $J[NO_2]$ and $J[O_3]$ comprised between 2 and 50 %, the maximum reduction being modelled in the aerosol plume. These modifications of photolysis frequencies result in an regional increase in the daytime concentration of NO_2 of 3–15 % and a decrease in the O_3 production near the surface comprised between 1 and 12 % during 8 August.

The photochemistry over the Moscow region has also been affected, especially during the arrival of the aerosol plume between 6 and 10 August 2010. Over this area, results indicate that $J[O_3]$ is more sensitive to the presence of particles (reduction of about 19 % per unit of AOT) than $J[NO_2]$ (reduction of about 10 % per unit of AOT), resulting in an increase of the ground NO_2 concentration of 4 % (per unit of AOT) and a small reduction of ozone of 2 % (per unit of AOT). The photochemistry is shown to be impacted along the boundary layer where aerosols are located with, for example, a 4–5 % O_3 reduction modelled during 9 August within the first two km of the atmosphere.

In terms of model performance, comparisons of simulations with air quality measurements at Moscow indicate that an explicit representation of aerosols interaction with photolysis rates tend to improve the estimation of the near-surface concentration of ozone and nitrogen dioxide, with some potential consequence for air quality prediction. For instance, the O_3 peak reduction when including aerosol feedback induces a non-negligible difference in the predicted exceedance of alert threshold during 8 August compared to the simulation without aerosol feedback, in coherence with measurements.

In addition, the impact of aerosols on photolysis rates is shown to have an influence on the formation of secondary aerosols, through the modification of the OH concentration. Over Moscow, the aerosol plume tends to decrease the daytime concentrations of sulphates and secondary organics up to 4–10 %, which result in a small reduction of the total particulate concentration (PM_{10}) of 1–2 % on average over the period. The results presented in this work, issued from a modelling exercise, are consistent with

ACPD
15, 7057–7087, 2015

those obtained in recent studies by combining model experiments and different sets of observations.

Recently, it has been suggested that some organic aerosols can absorb solar radiation, especially at the shorter visible and UV wavelengths (Zhong and Jang, 2011; Saleh et al., 2014). The methodology developed in this study provides a powerful tool to investigate the role of enhanced UV absorption by secondary organics on photochemistry at regional and urban scale.

Acknowledgements. Authors are grateful to the CRI at Lille 1, François Thieuleux at LOA and Anthony Ung at INERIS for their technical support. Olga Kislova at Mosecomonitoring (Moscow) is acknowledged for providing the surface air quality measurements used in this study. Authors would also like to thank Isabelle Chiapello at LOA for her fruitful scientific discussion. The CNES french spatial agency is acknowledged for its financial support.

References

Amin, N.: Effect of ozone on the relative yield of rice crop in Japan evaluated based on monitored concentrations, Water Air Soil Pollut., 225, 1–9, 2014. 7059

Beelen, R., Raaschou-Nielsen, O., Stafoggia, M., and co authors: Effects of long-term exposure to air pollution on natural-cause mortality: an analysis of 22 European cohorts within the multicentre ESCAPE project, Lancet, 383, 785–795, 2014. 7058

Bessagnet, B., Hodzic, A., Vautard, R., Beekmann, M., Cheinet, S., Honoré, C., Liousse, C., and Rouil, L.: Aerosol modeling with CHIMERE – preliminary evaluation at the continental scale, Atmos. Environ., 38, 2803–2817, 2004. 7061

Bessagnet, B., Menut, L., Curci, G., Hodzic, A., Guillaume, B., Liousse, C., Moukhtar, S., Pun, B., Seigneur, C., and Schulz, M.: Regional modeling of carbonaceous aerosols over Europe–focus on secondary organic aerosols, J. Atmos. Chem., 61, 175–202, doi:10.1007/s10874-009-9129-2, 2008. 7061

Bian, H., Han, S., Tie, X., Sun, M., and Liu, A.: Evidence of impact of aerosols on surface ozone concentration in Tianjin, China, Atmos. Environ., 41, 4672–4681, 2007. 7068

Guenther, A., Karl, T., Harley, P., Wiedinmyer, C., Palmer, P. I., and Geron, C.: Estimates of global terrestrial isoprene emissions using MEGAN (Model of Emissions of Gases and

ACPD
15, 7057–7087, 2015

Aerosols from Nature), Atmos. Chem. Phys., 6, 3181–3210, doi:10.5194/acp-6-3181-2006, 2006. 7062
Hauglustaine, D. A., Hourdin, F., Jourdain, L., Filiberti, M. A., Walters, S., Lamarque, J. F., and Holland, E. A.: Interactive chemistry in the Laboratoire de Météorologie Dynamique general circulation model: description and background tropospheric chemistry evaluation, J. Geophys. Res., 109, D04314, doi:10.1029/2003JD003957, 2004. 7062
Hodzic, A., Madronich, S., Bohn, B., Massie, S., Menut, L., and Wiedinmyer, C.: Wildfire particulate matter in Europe during summer 2003: meso-scale modeling of smoke emissions, transport and radiative effects, Atmos. Chem. Phys., 7, 4043–4064, doi:10.5194/acp-7-4043-2007, 2007. 7067
Honoré, C., Rouil, L., Vautard, R., Beekmann, M., Bessagnet, B., Dufour, A., Elichegaray, C., Flaud, J. M., Malherbe, L., Meleux, F., Menut, L., Martin, D., Peuch, A., Peuch, V. H., and Poisson, N.: Predictability of European air quality: assessment of 3 years of operational forecasts and analyses by the PREV'AIR system, J. Geophys. Res., 113, D04301, doi:10.1029/2007JD008761, 2008. 7059, 7070
Horowitz, L. W., Walters, S., Mauzeralles, D. Z., Emmonds, L. K., Rash, P. J., Granier, C., Tie, X., Lamarque, J. F., and Schultz, M. G.: A global simulation of tropospheric ozone and related tracers: description and evaluation of MOZART, version 2, J. Geophys. Res., 108, 4784, AAC 5-1-AAC 5-12, 2003. 7062
Hunova, I., Maly, M., Rezacova, J., and Branis, M.: Association between ambient ozone and health outcomes in Prague, Int. Arch. Occ. Env. Hea., 86, 89–97, 2014. 7059
Jenkin, M. E. and Clemitshaw, K. C.: Ozone and other secondary photochemical pollutants: chemical processes governing their formation in the planetary boundary layer, Atmos. Environ., 34, 2499–2527, 2000. 7059
Joseph, J. H., Wiscombe, W. J., and Weinman, J. A.: The delta-Eddington approximation for radiative flux transfer, J. Atmos. Sci., 33, 2452–2459, 1976. 7065
Junker, C. and Liousse, C.: A global emission inventory of carbonaceous aerosol from historic records of fossil fuel and biofuel consumption for the period 1860–1997, Atmos. Chem. Phys., 8, 1195–1207, doi:10.5194/acp-8-1195-2008, 2008. 7061
Kaiser, J. W., Heil, A., Andreae, M. O., Benedetti, A., Chubarova, N., Jones, L., Morcrette, J.-J., Razinger, M., Schultz, M. G., Suttie, M., and van der Werf, G. R.: Biomass burning emissions estimated with a global fire assimilation system based on observed fire radiative power, Biogeosciences, 9, 527–554, doi:10.5194/bg-9-527-2012, 2012. 7062

ACPD
15, 7057–7087, 2015

Konovalov, I. B., Beekmann, M., Kuznetsova, I. N., Yurova, A., and Zvyagintsev, A. M.: Atmospheric impacts of the 2010 Russian wildfires: integrating modelling and measurements of an extreme air pollution episode in the Moscow region, Atmos. Chem. Phys., 11, 10031–10056, doi:10.5194/acp-11-10031-2011, 2011. 7060

Lau, W. K. M. and Kim, K.-M.: The 2010 Pakistan flood and Russian heat wave: teleconnection of hydrometeorological extremes, J. Hydrometeorol., 13, 392–403, 2012. 7065

Lesins, G., Chylek, P., and Lohmann, U.: A study of internal and external mixing scenarios and its effect on aerosol optical properties and direct radiative forcing, J. Geophys. Res., 107, 4094, D11308, doi:10.1029/2004JD005463, 2002. 7063

Li, G., Bei, N., Tie, X., and Molina, L. T.: Aerosol effects on the photochemistry in Mexico City during MCMA-2006/MILAGRO campaign, Atmos. Chem. Phys., 11, 5169–5182, doi:10.5194/acp-11-5169-2011, 2011. 7059, 7071

Li, J., Wang, Z., Wang, X., Yamaji, K., Takigawa, M., Kanaya, Y., Pochanart, P., Liu, Y., Irie, H., Hu, B., Tanimoto, H., and Akimoto, H.: Impacts of aerosols on summertime tropospheric photolysis frequencies and photochemistry over Central Eastern China, Atmos. Environ., 45, 1817–1829, 2011. 7059

Lou, S., Liao, H., and Zhu, B.: Impacts of aerosols on surface-layer ozone concentrations in China through heterogeneous reactions and changes in photolysis rates, Atmos. Environ., 85, 123–138, 2014. 7059

Madronich, S. and Flocke, S.: The role of solar radiation in atmospheric chemistry, in: Handbook of Environmental Chemistry, Springer-Verlag, Heidelberg, Germany, 1–26, 1998. 7060, 7064, 7065

McMeeking, G. R., Morgan, W. T., Flynn, M., Highwood, E. J., Turnbull, K., Haywood, J., and Coe, H.: Black carbon aerosol mixing state, organic aerosols and aerosol optical properties over the United Kingdom, Atmos. Chem. Phys., 11, 9037–9052, doi:10.5194/acp-11-9037-2011, 2011. 7062

Mena-Carrasco, M., Carmichael, G. R., Campbell, J. E., Zimmerman, D., Tang, Y., Adhikary, B., D'allura, A., Molina, L. T., Zavala, M., García, A., Flocke, F., Campos, T., Weinheimer, A. J., Shetter, R., Apel, E., Montzka, D. D., Knapp, D. J., and Zheng, W.: Assessing the regional impacts of Mexico City emissions on air quality and chemistry, Atmos. Chem. Phys., 9, 3731–3743, doi:10.5194/acp-9-3731-2009, 2009. 7068

Menut, L., Bessagnet, B., Khvorostyanov, D., Beekmann, M., Blond, N., Colette, A., Coll, I., Curci, G., Foret, G., Hodzic, A., Mailler, S., Meleux, F., Monge, J.-L., Pison, I., Siour, G., Tur-

ACPD
15, 7057–7087, 2015

quety, S., Valari, M., Vautard, R., and Vivanco, M. G.: CHIMERE 2013: a model for regional atmospheric composition modelling, Geosci. Model Dev., 6, 981–1028, doi:10.5194/gmd-6-981-2013, 2013. 7059, 7061

Miller, M. R., Shaw, C. A., and Langrish, J. P.: From particles to patients: oxidative stress and the cardiovascular effects of air pollution, Future Cardiology, 8, 577–602, 2012. 7058

Péré, J. C., Mallet, M., Bessagnet, B., and Pont, V.: Evidence of the aerosol core-shell mixing state over Europe during the heat wave of summer 2003 by using CHIMERE simulations and AERONET inversions, Geophys. Res. Lett., 36, L09807, doi:10.1029/2009GL037334, 2009. 7060

Péré, J. C., Mallet, M., Pont, V., and Bessagnet, B.: Evaluation of an aerosol optical scheme in the chemistry-transport model CHIMERE, Atmos. Environ., 44, 3688–3699, 2010. 7060, 7062

Péré, J. C., Bessagnet, B., Mallet, M., Waquet, F., Chiapello, I., Minvielle, F., Pont, V., and Menut, L.: Direct radiative effect of the Russian wildfires and its impact on air temperature and atmospheric dynamics during August 2010, Atmos. Chem. Phys., 14, 1999–2013, doi:10.5194/acp-14-1999-2014, 2014. 7060, 7062, 7063, 7064, 7068, 7071

Popovicheva, O., Kistler, M., Kireeva, E., Persiantseva, N., Timofeev, M., Kopeikin, V., and Kasper-Giebl, A.: Physicochemical characterization of smoke aerosol during large-scale wildfires: extreme event of August 2010 in Moscow, Atmos. Environ., 96, 405–414, 2014. 7060

Real, E. and Sartelet, K.: Modeling of photolysis rates over Europe: impact on chemical gaseous species and aerosols, Atmos. Chem. Phys., 11, 1711–1727, doi:10.5194/acp-11-1711-2011, 2011. 7059, 7067, 7068, 7071

Saleh, R., Robinson, E. S., Tkacik, D. S., Ahern, A. T., Liu, S., Aiken, A. C., Sullivan, R. C., Presto, A. A., Dubey, M. K., Yokelson, R. J., Donahue, N. M., and Robinson, A. L.: Brownness of organics in aerosols from biomass burning linked to their black carbon content, Nat. Geosci., 7, 647–650, 2014. 7073

Seinfeld, J. H. and Pandis, S. N.: Atmospheric Chemistry and Physics. From Air Pollution to Climate Change, 2nd edn., Wiley-Interscience publication, 2006. 7059

Vautard, R., Beekmann, M., Roux, J., and Gombert, D.: Validation of a hybrid forecasting system for the ozone concentrations over the Paris area, Atmos. Environ., 14, 2449–2461, 2001. 7061

ACPD
15, 7057–7087, 2015

Vautard, R., Bessagnet, B., Chin, M., and Menut, L.: On the contribution of natural aeolian sources to particulate matter concentrations in Europe: Testing hypotheses with a modeling approach, Atmos. Environ., 39, 3291–3303, 2005. 7061

Vester, B. P., Ebert, M., Barnert, E. B., Schneider, J., Kandler, K., Schütz, L., and Weinbruch, L.: Composition and mixing state of the urban background aerosol in the Rhein-Main area (Germany), Atmos. Environ., 41, 6102–6115, 2007. 7062

Wai, K. M. and Tanner, P. A.: Variations of aerosol properties due to regional source contributions and impacts on ozone levels: a study in a south China city, Environ. Chem., 7, 359–369, 2010. 7059, 7068

Wu, X., Seigneur, C., and Bergström, R.: Evaluation of a sectional representation of size distributions for calculating aerosol optical properties, J. Geophys. Res., 101, 19277–19283, 1996. 7063

Wu, Z. P. and Wang, Y. P.: Electromagnetic scattering for multilayered spheres: Recursive algorithms, Radio Sci., 26, 1393–1401, 1991. 7063

Zhong, M. and Jang, M.: Light absorption coefficient measurement of SOA using a UV-Visible spectrometer connected with an integrating sphere, Atmos. Environ., 45, 4263–4271, 2011. 7073

Zvyagintsev, A. M., Ivanova, N. S., Blyum, O. B., Kotel'nikov, S. N., Kruchenitskii, G. M., Kuznetsova, I. N., and Lapchenko, V. A.: Ozone content over the Russian Federation in the third quarter of 2010, Russ. Meteorol. Hydrol., 35, 785–789, 2010. 7060

ACPD
15, 7057–7087, 2015

Table 1. Statistical comparisons between the near-surface concentrations of NO_2 and O_3 simulated with and without aerosols and measured at Moscow by an air quality station. Mod. and Obs. are the period-averaged modelled and observed concentration. Corr. and RMSE are the temporal correlation and the root mean square error.

	NO_2				O_3			
	Mod. ($\mu g\,m^{-3}$)	Obs. ($\mu g\,m^{-3}$)	Corr.	RMSE ($\mu g\,m^{-3}$)	Mod. ($\mu g\,m^{-3}$)	Obs. ($\mu g\,m^{-3}$)	Corr.	RMSE ($\mu g\,m^{-3}$)
with	14	70	0.22	66	129	66	0.46	82
without	13	70	0.21	67	134	66	0.42	88

ACPD
15, 7057–7087, 2015

Table 2. Same as in Table 1 but for daily maximum values.

	NO_2				O_3			
	Mod. ($\mu g\,m^{-3}$)	Obs. ($\mu g\,m^{-3}$)	Corr.	RMSE ($\mu g\,m^{-3}$)	Mod. ($\mu g\,m^{-3}$)	Obs. ($\mu g\,m^{-3}$)	Corr.	RMSE ($\mu g\,m^{-3}$)
with	32	90	0.60	66	180	161	0.19	48
without	31	90	0.60	67	185	161	0.16	54

ACPD
15, 7057–7087, 2015

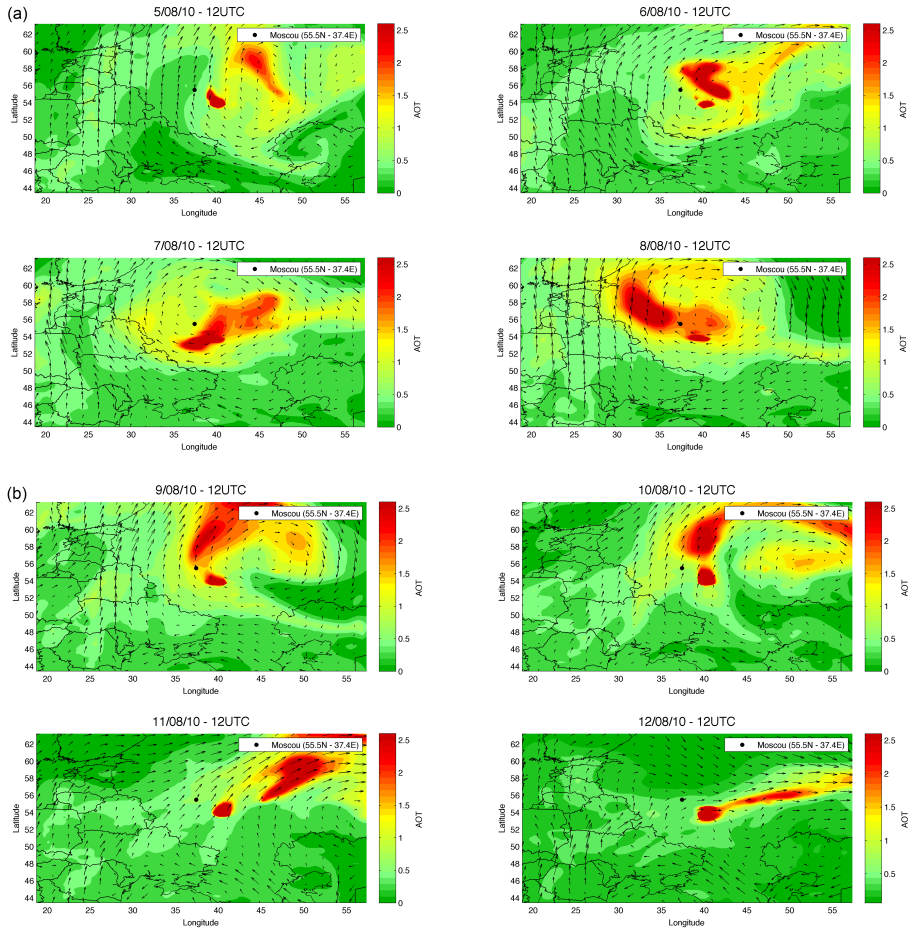

Figure 1. Geographic distribution of the AOT (at midday) over Eastern Europe from 5 to 12 August 2010 modelled by CHIMERE (at 400 nm). Horizontal wind at 850 hPa simulated by WRF is also indicated.

ACPD
15, 7057–7087, 2015

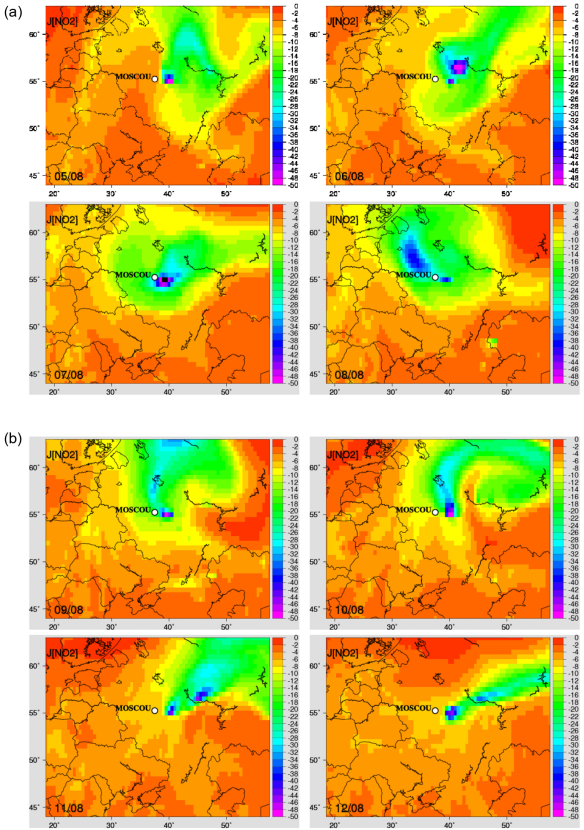

Figure 2. Geographic distribution of the modelled diurnal-averaged percentage changes in $J[NO_2]$ due to the presence of aerosols.

ACPD
15, 7057–7087, 2015

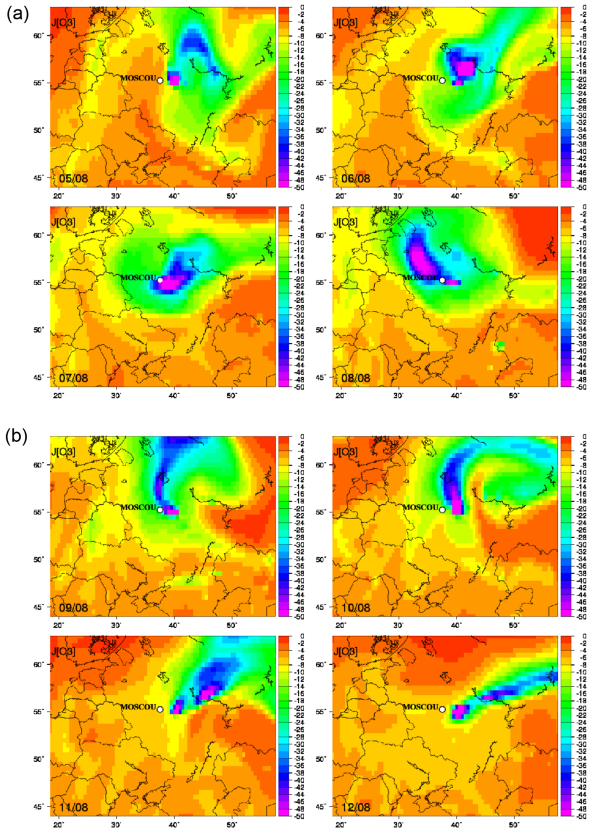

Figure 3. Geographic distribution of the modelled diurnal-averaged percentage changes in $J[O_3]$ due to the presence of aerosols.

ACPD
15, 7057–7087, 2015

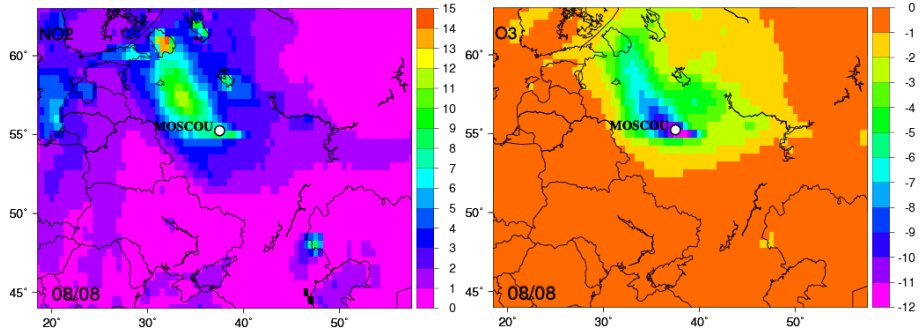

Figure 4. Geographic distribution of the diurnal-averaged percentage changes in the near-surface concentration of NO_2 (left) and O_3 (right) for the 8 August 2010, due to the presence of aerosols.

ACPD
15, 7057–7087, 2015

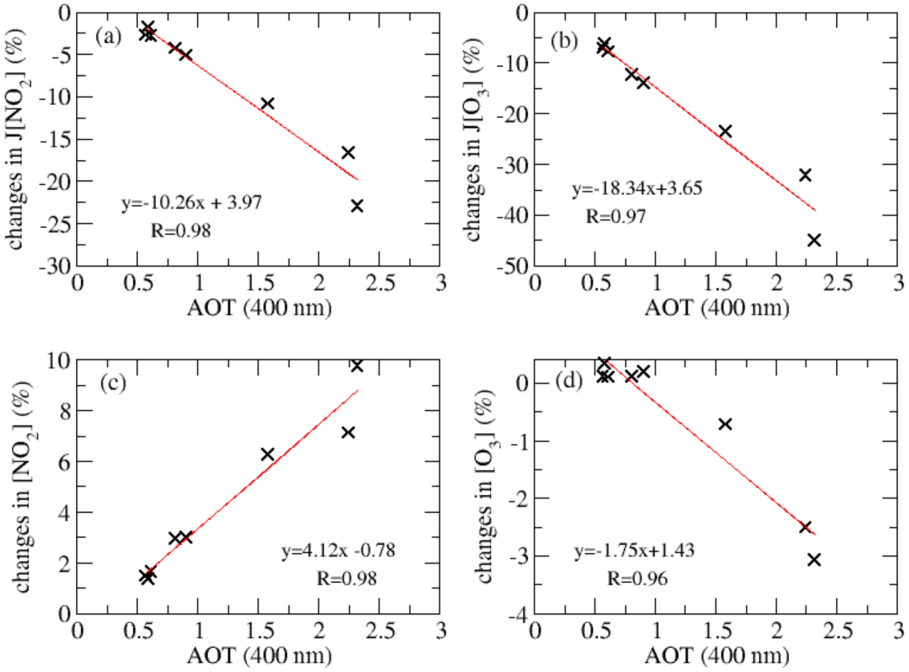

Figure 5. Percentage changes (at midday) in the photolysis frequencies and concentrations of nitrogen dioxide and ozone over Moscow as a function of modelled AOT (440 nm).

ACPD
15, 7057–7087, 2015

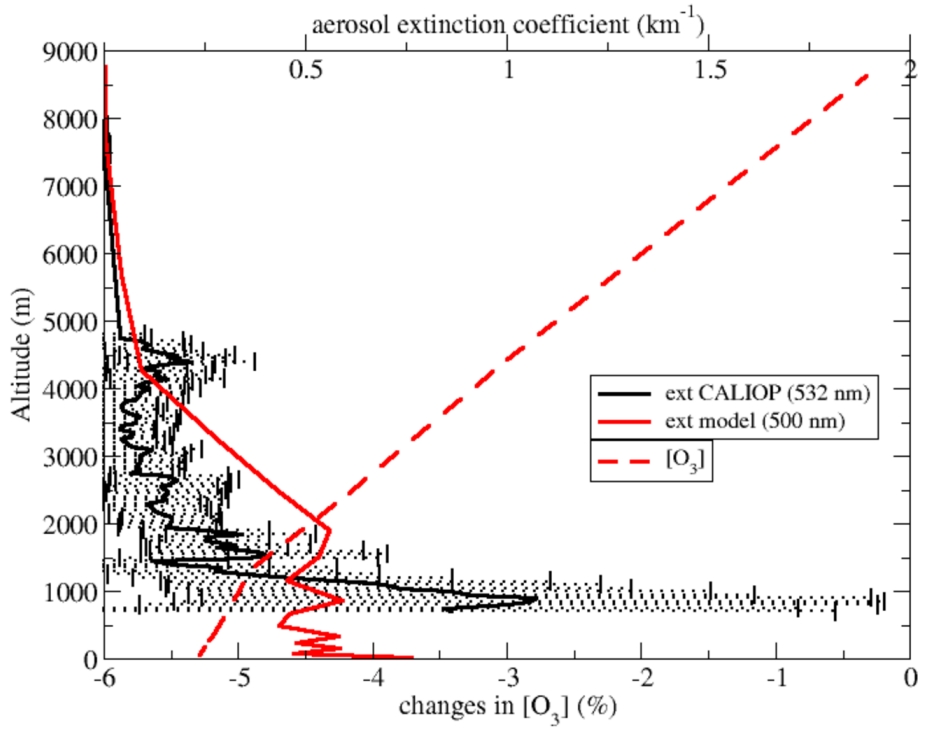

Figure 6. Vertical profile of the diurnal-averaged percentage changes in the ozone concentration at the north of Moscow (59.9° N, 37.6° E) for the 9 August. The aerosol extinction coefficient (in km^{-1}) modelled by CHIMERE and measured by CALIOP at midnight is also indicated.

ACPD
15, 7057–7087, 2015

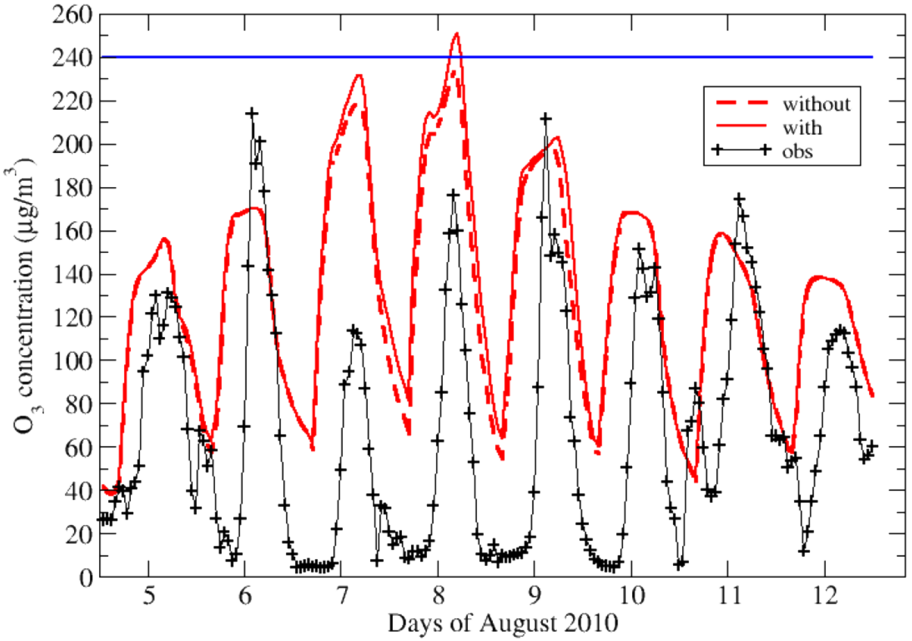

Figure 7. Temporal evolution (between 5 and 12 August 2010) of the near-surface ozone concentration (in µg m^{-3}) modelled with and without aerosol feedback along with corresponding observations at the Moscow monitoring station. The European alert threshold of 240 µg m^{-3} is also indicated by a straight line.

ACPD
15, 7057–7087, 2015

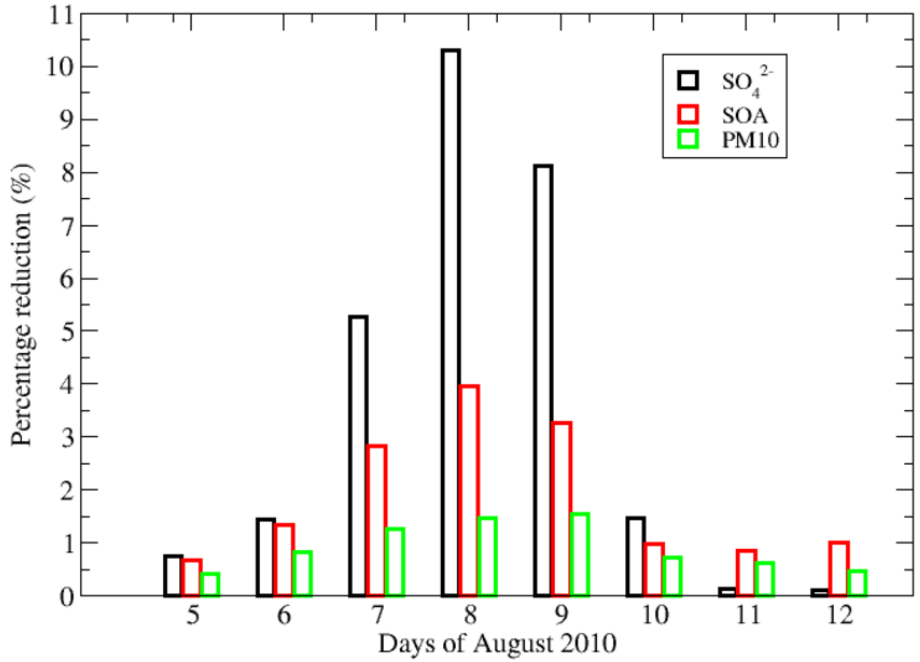

Figure 8. Diurnal-averaged percentage reduction of the near-surface concentration of sulphates, secondary organic aerosols and PM_{10} over Moscow due to the aerosol feedback.

ACPD
15, 7057–7087, 2015